Advances in Water Resources 55 (2013) 178–189

Contents lists available at SciVerse ScienceDirect

Advances in Water Resources

journal homepage: www.elsevier.com/locate/advwatres

# Sensitivity of turbulent fluxes to wind speed over snow surfaces in different climatic settings

Ruzica Dadic [a,*], Rebecca Mott [b], Michael Lehning [b,c], Marco Carenzo [d], Brian Anderson [a], Andrew Mackintosh [a]

[a] Antarctic Research Centre, Victoria University of Wellington, P.O. Box 600, Wellington, New Zealand
[b] WSL Institute for Snow and Avalanche Research, SLF, Flüelastrasse 11, 7260 Davos, Switzerland
[c] School of Architecture, Civil and Environmental Engineering, EPFL, Lausanne, Switzerland
[d] Institute of Environmental Engineering, ETH Zürich, Switzerland

ARTICLE INFO

*Article history:*
Available online 7 July 2012

*Keywords:*
Turbulent uxes sensitivity
Energy balance
Wind speed
Snow and Ice
Glacier mass balance

ABSTRACT

Local wind speed variations influence the energy and mass fluxes over snow through snow accumulation, sublimation of drifting and blowing snow, or variations in turbulent fluxes over static snow and ice surfaces. We use idealized model experiments to analyze the sensitivity of turbulent fluxes over static snow surfaces to variations in wind speed under different climatic conditions. We find that the sensitivity (change in the turbulent flux per change of unit wind speed) increases with increasing air temperature and relative humidity. The sensitivity of turbulent fluxes to wind speed is highest when the stability parameter $\zeta = 1$, which occurs at wind speeds typical for glacierized catchments (3–5 m $s^{-1}$), and exponentially decreases either side of that range. That peak in sensitivity is caused by atmospheric stability corrections in the model, and occurs independently of the flux-profile relationships we tested. Our results quantify the significant effect of local wind speed variations on turbulent fluxes over snow and ice and can be used to estimate potential model uncertainties in different climates, especially for the typical assumption in distributed hydrological models that the wind speed is spatially constant.



## 1. Introduction

In mountainous regions, changes in topography cause acceleration or deceleration of air masses and lead to increased wind velocity over ridges and reduced velocities in lee slopes and terrain depressions. Local winds influence the energy and mass fluxes over snow and ice surfaces through different processes. Snow accumulation and erosion is the obvious and probably most discussed process in context with local wind speed variations (e.g., [1–6]). Another process that is strongly dependent on wind speed is the sublimation of blowing snow due to increased surface area of blowing snow (e.g., [7–12]). A less obvious process is the influence of local wind speed variations on turbulent heat exchange over static surfaces of snow and ice (e.g., [13–19]). Local wind speed variations lead to spatially varying turbulent heat fluxes, which can be significantly under- or overestimated if the spatial variations in wind speed are neglected. While this is qualitatively known, most applications of distributed hydrological energy-balance (EB) models neglect the systematic influence of local terrain on wind speed variations. These spatial variations influence snow and ice temperatures and hence the onset and magnitude of snowpack melt.

For most of the year, the snow surface is colder than the overlying air and the turbulent fluxes transport heat from the air to the snow. In areas with high wind speed, high sensible heat flux can increase heat transfer from the air to the surface and lead to an earlier (both in the day and in the season) onset of melt [17,20]. In very humid conditions, the latent heat flux is also directed toward the snow surface, either through inverse sublimation or through rain on snow events [21], which further increases the energy flux into the snow. In very dry conditions, the latent heat flux is directed away from the surface, causing sublimation, and may offset some of the sensible heat flux. The sensible heat flux is usually larger than the latent heat flux and the sum of the two is therefore almost always positive toward the surface. In areas with low wind speed, the sensible heat flux is small and less heat is transported toward the surface. These areas experience less melt and a later melt onset. Fujita et al. [18] and Mott et al. [20,22] found that the process of decreased turbulent heat fluxes over sheltered snow patches or small glaciers can be, along with enhanced accumulation in these areas [23,24,4], an important factor for the survival of small glaciers and snow patches.

Marks and Dozier [15] and Marks and Winstral [16] found that higher wind speed at wind-exposed sites leads to a significant increase (~30%) in turbulent fluxes and therefore to higher mass fluxes than at sheltered sites with low wind speed. The results of

* Corresponding author.
*E-mail address:* ruzica.dadic@vuw.ac.nz (R. Dadic).

0309-1708/$ - see front matter © 2012 Elsevier Ltd. All rights reserved.
http://dx.doi.org/10.1016/j.advwatres.2012.06.010

Marks and Winstral [16] further show that the sensible heat fluxes are the most important factor contributing to snowmelt at unsheltered sites, while radiation was the most important factor at sheltered sites. The average wind speed for their unsheltered and their sheltered sites were 4–5 m $s^{-1}$ and 2 m $s^{-1}$, respectively, and this twofold difference leads to an almost 10-fold increase in the net turbulent flux at the unsheltered site, which already had less snow accumulation due to less snow deposition and more snow drift because of higher wind speeds. The combination of less snow accumulation and more turbulent heat fluxes leads to an earlier melt-out of the snowpack at wind-exposed sites. Marks et al. [21] show that the effect of enhanced turbulent fluxes at sites with high wind speed becomes even more important during warm storms, where relative humidity and air temperature are high and both latent and sensible heat flux are directed toward the surface. They show that during a storm in the Central Cascade Mountains of Oregon, 60–90% of the melt (235 mm water equivalent (w.e.)) at unsheltered sites came from turbulent heat fluxes, while it was only about 35% (48 mm w.e.) at the sheltered site.

Winstral and Marks [25] and Pohl et al. [17] discuss the basin-wide spatial variability of turbulent fluxes using modeled wind speeds from empirical wind-topography relationships [2,25]. A recent study by Mott et al. [19] investigated snow ablation in an Alpine catchment, used wind fields from a meteorological model to drive an energy balance model and showed that during late ablation season, turbulent fluxes contribute 35% of the net melt energy in areas that have above-average wind velocities. These studies demonstrate the relevance of the correct spatial distribution of wind velocity for the energy balance and snow ablation at wind-exposed or wind-sheltered areas.

None of the above studies discuss the sensitivity of turbulent fluxes with respect to wind speed. Greuell and Oerlemans [14] discussed the sensitivity of turbulent fluxes to wind speed for an average July climate in the European Alps, at the elevation of the glacier equilibrium line. They concluded that, for the particular climatic setting and given surface conditions (bare glacier-ice), turbulent fluxes linearly increase with wind speed above 4–5 m $s^{-1}$ and completely disappear below 3 m $s^{-1}$. Because the sensitivity analysis was not the main goal of their work, they limit the discussion of sensitivity of turbulent fluxes to wind speed to the one climatic condition. Furthermore, the log linear relationship, as used by Greuell and Oerlemans [14], does not allow significant fluxes to occur at strong stability (low wind speeds), and thus the fluxes completely disappear below 3 m $s^{-1}$. The lack of fluxes at strong stability can lead to a decoupling of the surface and the overlying air and trigger a runaway surface cooling in a model [26–28]. Most studies suggest that the log-linear law underestimates the surface flux in very stable conditions, as they often occur over snow and ice surfaces (e.g., [29–33]).

The sensitivity of turbulent fluxes to wind speed varies in different environments, because of the strong feedback between turbulent fluxes and surface temperature/longwave outgoing radiation. To quantify the sensitivity in different environments, we extend the analysis of Greuell and Oerlemans [14] and address the influence of wind speed on turbulent fluxes for different combinations of air temperature and relative humidity, which should represent a range of climatic conditions (e.g., different regions, seasons and elevations). We further use a flux-profile relationship that is valid under very stable conditions [34], so we can asses the sensitivity under low wind speeds and strong stability. First, we use idealized model runs from an energy balance model during a 24 h modeling period with stable stratification to estimate the sensitivity of turbulent fluxes to wind speed for different combinations of air temperature and relative humidity. Second, we address the sensitivity of the turbulent fluxes associated with variations of wind speed in alpine terrain, and its influence on the energy balance in a more realistic experiment. For that, we run the model for the basin of Haut Glacier d'Arolla for the 2007 winter, spring and summer seasons, using spatially modeled wind speed, measured meteorological variables and evolving albedo. We discuss the sensitivity to wind speed in the full spatial domain and the effect of the assumption of spatially uniform wind speed, which is common for energy balance calculations in mountain regions. Our results show that local wind field variations have largest implications for the spring and summer seasons, where enhanced turbulent fluxes over areas with high wind speed lead to an earlier melt onset (earlier in the season as well as earlier in the day) and to more melt.

## 2. Model description and setup

The energy-balance model that we use for this work (SnowDEM [35]), has previously been used by Corripio [35], Dadic et al. [36,37] and Pellicciotti et al. [38]. We ran SnowDEM as a distributed model with an hourly time step on a 10 × 10 meter grid for the catchment of the Haut Glacier d'Arolla in southwestern Switzerland. The model calculates the net energy flux at the snow surface:

$$\Delta Q_S + \Delta Q_M = I_G(1-\alpha) + L\downarrow + L\uparrow + H + E + Q_G + Q_R \quad (1)$$

where $\Delta Q_S$ is the transport of sensible heat into or out of the snowpack and $\Delta Q_M$ is the latent heat change due to melting or refreezing, $I_G$ is the incoming shortwave radiation, $\alpha$ is the albedo, $L\downarrow$ is the downward flux of longwave radiation, $L\uparrow$ is the upward flux of longwave radiation, $H$ and $E$ are the turbulent sensible and latent heat fluxes, $Q_G$ is subsurface heat flux and $Q_R$ is the heat supplied by precipitation. The fluxes are positive toward the snow surface and negative toward the atmosphere. The model details for the radiative fluxes and the shading by surrounding topography are described in Corripio [35]. To model turbulent fluxes, surface temperature is required as a boundary condition. We calculated the surface temperatures following the model description in Corripio [35]. The feedback between the surface temperature and turbulent fluxes is a key factor for our sensitivity analysis. We can therefore not solve for the sensitivity of the turbulent fluxes analytically, without using an energy balance model.

### 2.1. Turbulent flux modeling

The turbulent fluxes were modeled using the bulk method, which assumes logarithmic profile shapes for mean wind speed ($u$), air temperature ($T_a$) and relative humidity ($RH$) in a neutrally stratified atmosphere, but where non-neutral atmospheric conditions cause deviations from those ideal profiles and can be described by stability correction functions [39]. These deviations are usually estimated using flux-profile relationships, which are functions of atmospheric stability and relate the fluxes of momentum, sensible heat and water vapor to their mean gradients. The most common way to formulate the deviations from neutral conditions is to incorporate empirical corrections functions to the MO (Monin–Obukhov) similarity theory [40]. Monin and Obukhov [40] suggested that the dimensionless turbulence characteristics in the surface layer depend solely on the friction velocity $u_*$, the measurement height $z$, the displacement length $d_0$ (in case of vegetation), the air density $\rho$ and the buoyancy flux (the production rate of turbulent energy resulting from the work of buoyancy forces) [34]. These key parameters can be combined into one dimensionless variable $\zeta$. $\zeta$ is used as the stability parameter and is a function of the Obukhov length $L$, measurement height $z$ [m] and displacement length $d_0$.

$$\zeta = \frac{z - d_0}{L} \quad (2)$$

$$L = \frac{u_*^3 \rho}{kg\left[\frac{H}{T_a c_p} + 0.61\frac{E}{L_e}\right]} \tag{3}$$

$$u_* = \frac{uk}{\ln\frac{z-d_0}{z_0} - \Psi_m(\zeta)} \tag{4}$$

The Obukhov length $L$ is a function of the friction velocity $u_*$, in which $k$ is the von Kármán constant (0.4), $z_0$ the roughness length for momentum (m) and $\Psi_m(\zeta)$ the stability correction function for momentum. The Obukhov length $L$ is further a function of air density $\rho$ (kg m$^{-3}$), acceleration of gravity $g$ (9.81 m s$^{-2}$), specific heat of dry air at constant pressure $c_p$ (1004.67 J kg$^{-1}$ K$^{-1}$), the sensible heat flux $H$ [W m$^{-2}$], the latent heat flux $E$ (W m$^{-2}$) and the latent heat of evaporation $L_e$ (J kg$^{-1}$). Including stability correction functions for sensible heat flux $\Psi_h(\zeta)$ and for latent heat flux $\Psi_q(\zeta)$, $H$ and $E$ can then be calculated as

$$H = \frac{ku_*\rho c_p(\Theta_a - \Theta_s)}{\ln\frac{z-d_0}{z_h} - \Psi_h(\zeta)} \tag{5}$$

$$E = \frac{ku_*\rho L_e(q_a - q_s)}{\ln\frac{z-d_0}{z_q} - \Psi_q(\zeta)} \tag{6}$$

with $\Theta_a$ (K) being potential temperature at measurement height $z$ (m), $\Theta_s$ (K) potential temperature at the snow surface, $q_a$ (g kg$^{-1}$) specific humidity of air at measurement height $z$ (m), $q_s$ (g kg$^{-1}$) specific humidity of air over snow, $z_h$ (m) roughness length for sensible heat, $z_q$ (m) roughness length for water vapor. The stability correction functions (profile functions) $\Psi(\zeta)$ are vertically integrated forms of the flux-profile relationships (gradient functions) $\phi(\zeta)$ [41]. The flux-profile relationships for wind speed ($\phi_m$), potential temperature ($\phi_h$) and relative humidity ($\phi_q$) depend on $\zeta$ and are referred to as the universal similarity functions (or non-dimensional gradients of wind speed, potential temperature or relative humidity). The form of $\phi$ has to be experimentally determined and there are many different forms found in the literature. Summaries can be found in Dyer [42], Yaglom [43] and Andreas [44]. For unstable conditions $\zeta \leqslant 0$, we used the Businger–Dyer relations [45,46]:

$$\phi_m^2(\zeta) = \phi_h(\zeta) = \phi_q(\zeta) = (1 - 16\zeta)^{-1/2} \tag{7}$$

For weakly stable conditions $0 \leqslant \zeta \leqslant 1$, we used the log-linear profiles, also known as Businger–Dyer [40,45,46], which are discussed in detail by Zilitinkevich and Chalikov [47], Businger et al. [48] and Yaglom [43]. For strong stability $\zeta > 1$ (high $T_a$ and low $u$), we used the extension of the log-linear profile that was suggested by Webb [30] and Kondo et al. [31] and was proposed for practical flux computations by Brutsaert [34]:

$$\phi_m(\zeta) = \phi_h(\zeta) = \phi_q(\zeta) = \begin{cases} 1 + \beta\zeta & \text{for } 0 < \zeta < 1 \\ 6 & \text{for } \zeta > 1 \end{cases} \tag{8}$$

with $\beta = 5$ [30,42,49,34,50]. The integrated forms $\Psi(\zeta)$ of $\phi(\zeta)$ for unstable conditions (Eq. (7)) can be found in Brutsaert [34, p. 70]. The integrated forms $\Psi(\zeta)$ of $\phi(\zeta)$ for stable conditions (Eq. (8)) can be found in Sharan [51], and are given here

$$\Psi_m(\zeta) = \Psi_h(\zeta) = \phi_q(\zeta) = \begin{cases} -\beta\zeta & \text{for } 0 < \zeta < 1 \\ -\beta - \beta\ln(\zeta) & \text{for } \zeta > 1 \end{cases} \tag{9}$$

Flux-profile relations for very stable conditions $\zeta \geqslant 1$ are not well understood. Measurements of turbulence under very stable conditions are harder to obtain because the mean flow is non-stationary, as opposed to the continuous flow under weakly stable conditions. The non-stationary flow leads to intermittent turbulence, that is "characterized by brief episodes of turbulence with intervening periods of relatively weak or unmeasurably small fluctuations" [52] (see also: [53,54,27,55]). The log-linear relationship does not allow for significant turbulence under strongly stable conditions. Therefore, a number of studies have been dedicated to finding flux-profile relationships that are valid under very stable conditions (e.g., [30,31,56,34,57,54,58,59]). We have tested three additional flux-profile functions which account for strong stability (Lettau [56], Holtslag and DeBruin [57], Cheng and Brutsaert [58]) and found that the sensitivity of the turbulent fluxes is comparable for all functions and that our results are therefore robust. Eqs. (2)–(8) cannot be uniquely solved analytically and are therefore solved iteratively [34,60].

### 2.2. Model setup for sensitivity analysis for different climatic conditions

We define sensitivity as the partial derivative of the turbulent flux with respect to wind speed, i.e., the change in the turbulent flux per change of unit wind speed. To estimate the sensitivity of turbulent fluxes to wind speed, we ran the energy balance model during a 24 h period, using meteorological data from the automatic weather station AWS1 (location in Fig. 5c) on January 30th 2007 as model input. That particular day was chosen because it had no clouds (zero cloud cover assumption for all model runs) and the variations in air temperature and relative humidity were relatively small (Fig. 1). The average temperature and relative humidity for 30 January 2007 at AWS1 were −4.6 °C and 31%, respectively. We evaluated the turbulent fluxes at one point in the catchment (2800 m.a.s.l., diamond in Fig. 5c), to which we will refer to as point SA. To extrapolate the temperature from AWS1 to SA, we used an air temperature lapse rate of −0.002 K m$^{-1}$, which leads to an average temperature of −4.2 °C at SA. The variations in relative humidity due to the 0.4 K temperature difference are negligible. To extend the sensitivity analysis to different climatic conditions, we varied the measured temperature by ±10 K (in steps

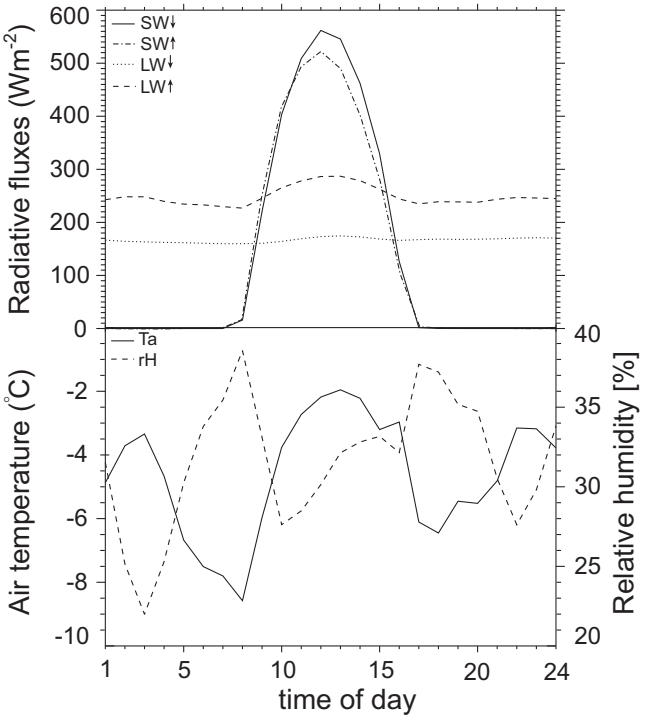


**Fig. 1.** Meteorological data from automatic weather station AWS1 (for location, see Fig. 5c), on January 30th 2007, was used as model input for the 24-h model experiments.

of 10 K) and the measured relative humidity by +30% and +60% (in steps of 30%). The combinations of the air temperature (−14.2 °C, −4.2 °C, +5.8 °C) and relative humidity (31%, 61%, 91%) variations results in 9 different climatic conditions, which are commonly found in a range of alpine regions during different seasons and at different elevations. The model was run for each climatic condition with temporally uniform wind speed of 1, 2, 3, 4, 5, 6, 9, 12, 15, 18 and 21 m $s^{-1}$.

To eliminate feedback effects on the turbulent fluxes through temporal changes of snow properties, we used the following input/boundary conditions for all model runs: (1) at timestep $t = 0$, the snow amount is 500 mm w.e., (2) snow density ($\rho_s = 300$ kg $m^{-3}$), albedo ($\alpha = 0.9$) and wind speed do not vary in time, (3) $z_0$ does not vary in time and is 0.001 m, which is an accepted value for mountainous regions (e.g., [61,62,33]). The insolation was kept the same for all model runs (Fig. 1). We are aware that the peak shortwave incoming radiation values in summer are almost twice as big as those in winter (which we used in this study), but changing the insolation values for model runs with summer Ta/rH-conditions would lead to changes in turbulent fluxes and feedbacks with the surface temperature, and we would not be able to isolate the sensitivity due to changes in air temperature and relative humidity alone. We additionally ran the model assuming neutral stratification and omitting the stability correction, so we can estimate what part of the sensitivity is caused by the stratification correction and what part is due to surface-temperature/longwave radiation feedback.

For the discussion of the results, we use the 24 h average value of each flux at SA (diamond in Fig. 5c). Because all our model runs are made for a clear sky day with negative net longwave radiation, we never have enough surface warming to cause unstable stratification, and do not discuss the sensitivity for unstable conditions. Over snow/ice surfaces, stable stratification is more common than unstable stratification, especially during melting conditions.

### 2.3. Model setup for the sensitivity analysis at the basin scale

To estimate the uncertainties in turbulent fluxes associated with spatial variations in wind speed in a more realistic spatial experiment with measured meteorological variables and evolving albedo, we ran the distributed energy balance model for the basin of Haut Glacier d'Arolla for the 2007 winter, spring and summer seasons. The model setup was as in Dadic et al. [37], except that for the study presented herein we used pre-modeled wind fields as model input to calculate the turbulent fluxes while omitting snow distribution due to wind, whereas Dadic et al. [37] used the pre-modeled wind fields to model preferential deposition of snow and assumed spatially uniform wind fields for turbulent flux modeling. We use the same wind fields as in Dadic et al. [37], which were modeled using the mesoscale atmospheric model ARPS [63,64]. We do not model wind fields for every timestep, but use pre-modeled wind fields for 14 typical wind situations in the basin of the Haut Glacier d'Arolla. We pick one of the 14 wind fields depending on the hourly wind speed and wind direction during the modeling period at a station outside of the basin. The station is integrated in the Intercantonal Measurement and Information System (IMIS) [65], and is at 3301 m asl, which was assumed to represent the synoptic wind patterns in the region, because it is located on a nearby ridge and minimally influenced by the local topography (for a more detailed description, see [37]). We did not apply a precipitation gradient, because it is unknown and not important in the context of this sensitivity study. The air temperature lapse rate was −0.002 K $m^{-1}$. The precipitable water was kept constant and the relative humidity was spatially varying due to temperature gradients. $z_0$ was spatially uniform with 0.001 m. The radiation and the shading by surrounding slopes is described by Corripio [35,66]. The snow albedo is parameterized using a weighted ageing-melt decaying curve (Corripio, personal communication) and details can be found in Dadic [67]. We ran the energy balance model for the time between January 1 and March 31, 2007 (day 1 and 90), between April 1 and May 31, 2007 (day 91 and 151) and between June 1 and September 28, 2007 (day 152 and 271) to estimate sensitivity of turbulent fluxes to wind speed in the winter, spring and summer season. The seasonally average values for wind speed, air temperature and relative humidity for the respective seasons at AWS1 (which was used as meteorological model input except for $u$, that was calculated with ARPS) are shown in Table 1. For the first set of model runs (MR1), we used the modeled wind speed (ARPS) and for the second set of model runs (MR2), we increased that wind speed uniformly over the catchment by 1 m $s^{-1}$. We define sensitivity as the difference between MR1 and MR2. We additionally ran the model assuming uniform wind speed from AWS1 (MR3), to asses how large the uncertainties in turbulent fluxes could be if local wind speed variations are neglected.

## 3. Results and discussion

In the first part of this section, we discuss the influence of wind speed on the turbulent fluxes and melt at one point for different climates, and discuss the implications of our results to different climatic regions (or elevations). In the second part, we discuss the uncertainties in turbulent fluxes associated with variations in modeled wind speed using a distributed approach in a glacierized catchment with measured meteorological variables and evolving albedo.

### 3.1. Sensitivity of turbulent fluxes to wind speed for different climatic conditions

In our experiments, the latent heat flux is positive (vapor deposition) for high relative humidity and negative (sublimation) for low relative humidity. For intermediate relative humidity (61%), latent heat flux becomes negative with increasing wind speed (Fig. 2a). The change from positive (inverse sublimation) to negative (sublimation) occurs between ∼8 m $s^{-1}$ (for $T_a = -14.2$ °C) and ∼14 m $s^{-1}$ (for $T_a = +5.8$ °C). This change occurs because higher wind speed increases the sensible heat flux and thus the snow surface temperature, which leads to an increase of specific humidity over snow ($q_s$) and hence affects the latent heat flux (Eq. (6)). The sensible heat flux is always positive and increases with increasing air temperature and decreasing relative humidity, because low relative humidity increases sublimation and cools the surface, which leads to larger temperature gradients and to increased sensible heat flux. Highest sensible heat fluxes are calculated for warm and dry climates, when air temperatures are high and snow surface temperatures are cooled by latent heat loss. High relative humidities decrease the sensible heat fluxes, because of increased latent heat flux toward the snow surface and vapor deposition, which warms up the surface temperature and subsequently leads to lower temperature gradients between the air and the surface. The sum of the turbulent sensible and latent fluxes (net turbulent flux) is highest for the warm and moist case, when both

**Table 1**
Seasonally averaged $u$, $T_a$ and $RH$ at automatic weather station AWS1 for 2007.

| day of 2007 | $u$ (m $s^{-1}$) | $T_a$ (°C) | $RH$ (%) |
|---|---|---|---|
| 1–90 | 3.1 | −7.9 | 65 |
| 91–151 | 2.8 | −1.9 | 73 |
| 152–271 | 2.5 | +2.5 | 75 |

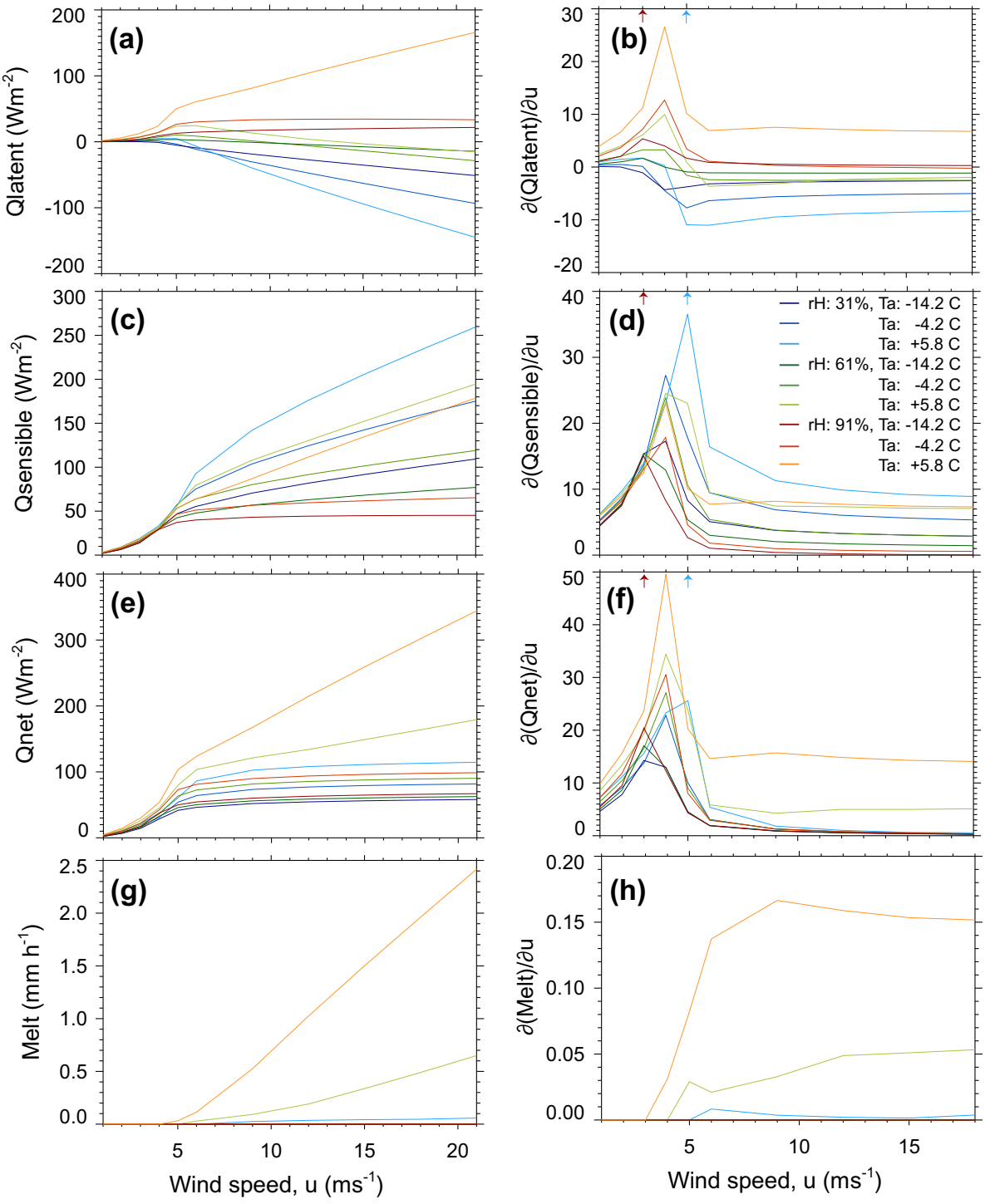


**Fig. 2.** Turbulent fluxes and melt (a,c,e,g) and sensitivities of turbulent fluxes and melt with respect to wind speed (b,d,f,h) as function of wind speed for nine different climatic conditions. Sensitivity is defined as the partial derivative of the turbulent flux with respect to wind speed. The red arrow in (b,d,f) shows the lower bound for $\zeta > 1$ (least stable climatic condition) and the blue arrow shows the upper bound for $\zeta > 1$ (most stable climatic condition).

fluxes are positive (Fig. 2e), and lowest for the cold and dry case, when the negative latent heat flux offsets the sensible heat flux.

Figs. 2b,d,f show the sensitivity of the turbulent fluxes and melt with respect to wind speed. Under very stable conditions, when $\zeta > 1$, the mean flow becomes non-stationary and the turbulent fluxes behave differently than for weakly stable conditions ($0 < \zeta < 1$). For both latent and sensible heat flux, the sensitivity is highest at $\zeta = 1$ (or $u = 3$–$5\ \mathrm{m\ s^{-1}}$). Below and above this range the sensitivity increases and decreases exponentially. It becomes almost constant, differing for the different climate conditions, for wind speeds above 8–10 $\mathrm{m\ s^{-1}}$, as the stratification approaches neutral. For all climatic conditions, $\zeta = 1$ occurs between 3 and 5 $\mathrm{m\ s^{-1}}$ (Fig. 2, peaks). This threshold is reached at 3 $\mathrm{m\ s^{-1}}$ for very moist ($rh = 91\%$) and cold ($T_a = -14.6\ ^\circ\mathrm{C}$) conditions (weak stability, Fig. 2b, d, f, red arrows), and at 5 $\mathrm{m\ s^{-1}}$ for very dry ($rh = 31\%$) and warm ($T_a = +5.6\ ^\circ\mathrm{C}$) conditions (strong stability, Fig. 2b, d, f, blue arrows). The dry and warm conditions lead to very stable stratifications, which requires higher wind speeds to mix the air.

The sensitivity of the turbulent fluxes to uncertainties in wind speed shows the same trends for all climatic conditions, but is highest for climatic conditions with highest fluxes. Both, latent and sensible heat fluxes (not sensitivities of the fluxes) increase with increasing wind speed (Fig. 2a, c, e), but the behavior changes at $\zeta = 1$. For $\zeta > 1$ (or $u < 3$–$5$ m s$^{-1}$) the increase is exponential and for $\zeta < 1$ (or $u > 3$–$5$ m s$^{-1}$) the increase is logarithmic.

Melt increases with relative humidity and increasing wind speed (Fig. 2g). Above 8–10 m s$^{-1}$, the increase with wind speed is almost linear, following the behavior of turbulent fluxes. The sensitivity of melt to changes in wind speed (Fig. 2h) strongly increases around 3–5 m s$^{-1}$ or $\zeta = 1$, after which it remains more or less constant for all wind speeds, reflecting sensitivity of the turbulent fluxes (Fig. 2f).

### 3.1.1. Neutral stratification assumption

When the stratification correction is omitted and the model forced to assume neutral stratification, the sensitivity of the turbulent fluxes to wind speed is highest at 1 m s$^{-1}$ and exponentially decreases with increasing wind speed (Fig. 3). For $\zeta < 1$ (or $u > 3$–$5$ m s$^{-1}$), the fluxes show the same pattern as with the stratification correction (logarithmic increase), albeit with the absolute values slightly higher when neutral stratification is assumed (Fig. 3). For $\zeta > 1$ (or $u < 3$–$5$ m s$^{-1}$), the neutral stratification leads to significantly higher fluxes in all climatic conditions and wind speeds as well as to a different behavior with increasing wind speed. While the fluxes calculated with the correction for stable stratification and $\zeta > 1$ show an exponential increase with wind speed (Fig. 2), the fluxes calculated assuming neutral stratification in the same wind speed range show a logarithmic increase with wind speed, which is caused by the surface temperature – longwave outgoing radiation feedback. We can therefore conclude that the modeled peaks in sensitivities (Fig. 2) are caused by the stratification correction in the model.

### 3.1.2. Implications for different climates: examples

Our analysis shows that the model sensitivity of turbulent heat fluxes to changes in wind speed varies for different climatic conditions. Turbulent fluxes are most sensitive to wind speed in maritime climates and regions with high relative humidity and high temperature, such as the Southern Alps in New Zealand or the Cascades and Olympic Mountains in the Northwestern United States. Gillet and Cullen [68] highlight the relevance of turbulent fluxes in maritime climates and show that turbulent fluxes over a maritime glacier in spring can account for an average of 45% of the surface energy balance, and that their contribution can increase to 72% during large melt events. We showed that for a climate with average $rh = 91\%$, $T_a = +5.4$ °C, $u > 4$ m s$^{-1}$ (with $\alpha = 0.9$), the underestimation of wind speed by only 1 m s$^{-1}$ (seasonal average) leads to an underestimation of melt of ~320 mm w.e. for a 90-day ablation season. This is ~250% of the total melt (from MR1) in regions where mean wind speed is around 5 m s$^{-1}$ and 10% of total melt in regions where mean wind speed is around 15 m s$^{-1}$. For wind speeds below 4 m s$^{-1}$, no melt occurs if wind speed is underestimated for the given conditions. For a more moderate relative humidity of 61% ($T_a = +5.4$ °C, $u = 4$ m s$^{-1}$, $\alpha = 0.9$), conditions as for example can be found in the European Alps or the Rocky Mountains after a fresh snowfall in spring, the underestimation of wind speed by 1 m s$^{-1}$ leads to an underestimation of melt by 65 mm w.e. (assuming an underestimation of melt of ~0.03 mm h$^{-1}$/m s$^{-1}$), which is ~70% of the total melt (from MR1) in regions of 5 m s$^{-1}$ and exponentially drops to 15% of total melt in regions of 15 m s$^{-1}$. The % contribution of turbulent fluxes to melt is likely overestimated in this scenario, because of the high albedo and low insolation values assumed, so the contribution from radiative fluxes is relatively small. However, Mott et al. [19] show that, even in moderate humidity climates like the Swiss Alps, turbulent fluxes can contribute 35% to the net melt energy in regions with above-average wind speed during the melt season. In dry regions, such as the semi-arid Andes in central Chile, where the average humidity in summer is low ~30–40% ($RH = 31\%$, $T_a = +5.4$ °C, $u = 4$ m s$^{-1}$, $\alpha = 0.6$) the underestimation of wind speed by 1 m s$^{-1}$ has almost no influence on the melt and leads to an underestimation of sublimation by 30 mm w.e. over a 90-day period. We have to bear in mind that these estimates are based on the conditions that we used for our analysis, which are high albedo and winter values for incoming solar radiation. The sensitivities will increase with decreasing albedo or increasing incoming solar radiation. For example, the summer temperatures in dry regions, such as the Andes, can be larger than the average summer temperature over glaciers in the European Alps: the higher temperature and the higher incoming solar radiation in proximity to the equator and generally higher altitudes in some of these regions are likely to cause a more positive energy balance and lead to greater melt. If these regions reach the melting point, the high sensitivity to wind speed at 3–5 m s$^{-1}$ (Fig. 2b, d, f) is likely to cause large underestimations of melt if wind speed is underestimated. Furthermore, the wind speed uncertainties in complex terrain are likely larger than 1 m s$^{-1}$, which also leads to an increase of the uncertainty in melt and sublimation due to wind speed.

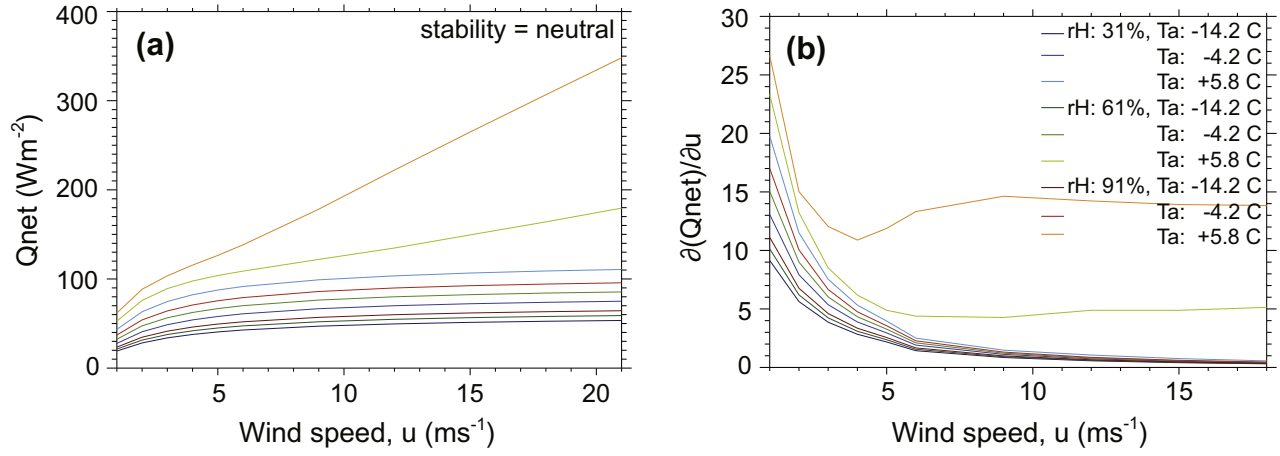


**Fig. 3.** Net turbulent fluxes (a) and sensitivity of the net turbulent fluxes (b) as function of wind speed for nine different climatic conditions under the assumption of neutral stratification.

For winter conditions with negative temperatures, the sensitivity of turbulent fluxes to uncertainties in wind speed is smaller, but can still cause significant errors in sublimation or inverse sublimation, if the wind speed uncertainties are large. For example, over a spot where the underestimation of wind speed is 4 m s$^{-1}$, $T_a = -4.6$ °C, $rH = 31\%$, and a winter season of 150 days, the underestimation of sublimation is 150 mm w.e.. In a humid climate with average $rH = 91\%$ the underestimation of inverse sublimation (deposition) is 230 mm w.e. This is most relevant over ridges and steep slopes, which already have less snow due to the preferential deposition of snow [3,5,4] and snow drift (e.g., [2,6,12]). The sublimation enhances the depletion of the snow cover in drier winters, and inverse sublimation in more humid springs (e.g., Table 1) increases snow temperatures and melt. The surface cooling/heating through the latent heat flux has a larger effect on the energy balance than the actual mass loss/gain through sublimation and vapor deposition [14].

### 3.2. Wind speed influence on the turbulent fluxes at the distributed scale

#### 3.2.1. A case study from Haut Glacier d'Arolla

Energy and mass balance models often assume spatially uniform wind speed when modeling snow/ice catchments, which can lead to uncertainties in turbulent fluxes. Our idealized model experiments (Section 3.1) showed that the largest sensitivities to wind speed occur for regions where wind speeds are between 3 and 5 m s$^{-1}$ in all climatic conditions, and that the uncertainties increase with increasing air temperature and relative humidity. In this non-idealized part of the sensitivity study, we used modeled wind fields, along with measured meteorological variables and evolving albedo, to estimate the potential errors in turbulent fluxes associated with spatial variations in wind speed in the catchment of Haut Glacier d'Arolla for the 2007 winter, spring and summer seasons. This experiment serves to put the theoretical sensitivity as discussed above in the spatial context of a glacierized mountain catchment. For the first set of model runs (MR1), we used the modeled wind speed and for the second set of model runs (MR2), we increased that wind speed uniformly over the whole catchment by 1 m s$^{-1}$. For the third set of model runs (MR3), we assumed a spatially uniform wind field. We first discuss the sensitivity as the difference between MR2 and MR1 and then discuss the difference between the runs that use the spatially uniform wind speed (MR3) and the modeled wind speed (MR1).

Fig. 4 shows the seasonally averaged difference in the sensible (a–c), latent (d–f) and net (g– i) heat flux between the two sets of model runs (MR2-MR1). The overlaid contours show the modeled wind speed for MR1. For the summer season, we only discuss glacierized areas, because the non-glacierized areas become snow- and ice-free in early summer, which changes the turbulent fluxes due to changes in surface conditions. By excluding non-glacierized areas, we also exclude regions of highest wind speed in our discussion of the summer season. As expected from our idealized model experiments (Fig. 2b, d, f), the sensitivity to wind speed is lowest for winter and increases with increasing temperature in spring and summer (Fig. 4). The sensitivity of the net turbulent flux is primarily influenced by the sensible heat flux, which has a larger magnitude than the sensitivity of the latent heat flux for most of the catchment.

The highest sensitivity of the turbulent heat fluxes for all seasons is for wind speeds between 3–6 m s$^{-1}$ (Fig. 4, contours). This is consistent with our idealized model experiments, where we observed peak sensitivity at $\zeta = 1$ or $u = 3$–5 m s$^{-1}$, and it shows that our model experiments can generally reproduce the patterns in sensitivity, despite idealized conditions. However, the idealized model experiments (Fig. 2) tend to overestimate the magnitude of the seasonal sensitivity (Fig. 4) when the average seasonal climate is assumed (Table 1). For example, the maximum sensitivity in the net turbulent flux in the idealized experiments, for $rH$ = 61% and $T_a = -4.6$ °C (close to spring conditions in (Table 1)), is ~25 W m$^{-2}$/m s$^{-1}$ at u = 4 m s$^{-1}$ (Fig. 2f), while in the seasonal model run the maximum sensitivity of the net turbulent flux occurs at the same wind speed, but is with 8 W m$^{-2}$/m s$^{-1}$ (Fig. 4h) one third of the value in the model experiment. This difference between the idealized conditions and seasonal model runs is likely caused by the non-linear effects of the temporal variability meteorological variables: for example, the average wind speed of 4 m s$^{-1}$ can be obtained by averaging between 2 and 6 m s$^{-1}$, which both have lower sensitivity than 4 m s$^{-1}$). Nevertheless, we show that the two main results from the idealized experiments, namely that: (1) there is a peak in sensitivity at $\zeta = 1$ ($u$ = 3–5 m s$^{-1}$); and (2) the sensitivity increases with increasing air temperature and increasing relative humidity, are valid for the catchment scale, and that those main results can be used to estimate turbulent flux uncertainties due to local wind speed variations in different climates.

Fig. 5 shows the seasonally averaged differences between a seasonally averaged spatially uniform wind speed (from AWS1, Table 1) and and the mean seasonal modeled wind speed (from MR1) for the winter, spring and summer seasons. The overlaid contours show the mean seasonal modeled wind speed (MR1). If we assume spatially uniform wind speed (as in MR3), we underestimate the wind speed everywhere but in lower part of the main glacier (Fig. 5, the glacier flows to the North). The ratio of under- and overestimated area depends on the location of the reference automatic weather station (AWS). If it is situated in an area with lower wind speed, then a model assuming uniform wind speed would underestimate the wind speed in large parts of the catchment. If it is situated in a windy spot, then assuming uniform wind speed would lead to an overestimation of wind speed in large parts of the catchment. Usually AWSs in glaciated catchments are situated in the proglacial valley and therefore likely to lead to an underestimation of wind speed for most of the catchment, if uniform wind speed is assumed. For this analysis, we used AWS1, which is situated neither in the valley floor nor on a ridge (Fig. 5c, AWS1). Assuming a uniform wind speed leads to an overestimation of wind speed on the glacier of up to 1.5 m s$^{-1}$, and to an underestimation over steep slopes and ridges of up to 5 m s$^{-1}$. Because ARPS has not been set-up to allow the development of katabatic winds, it likely underestimates wind speed over the lower part of the glacier.

Fig. 6 shows the average error of turbulent heat fluxes, if spatially uniform wind speed is assumed (MR3-M1). The contours in Fig. 6 show the average heat fluxes from MR1 and can be used to estimate the error in percent of the respective modeled flux. Even if the sensitivity is low for regions with high wind speed (Fig. 2), the underestimation of wind speed is high over these areas (Fig. 5), which leads to significant underestimation of turbulent heat fluxes over ridges and steep slopes. The sensible heat flux over ridges and steep slopes is underestimated by up to 30 W m$^{-2}$, which is ~50–100% of the modeled sensible heat flux in MR1, depending on the season. The error in the latent heat flux is much smaller (Fig. 6d–f), but so is the latent heat flux itself. The error is ~±1 W m$^{-2}$ over most of the catchment, except for the ridges and steep slopes, where it is overestimated by up to 10 W m$^{-2}$ (but still ~100% of the modeled latent heat flux in MR1). The net turbulent flux (Fig. 6g–i) is overestimated by up to 7 W m$^{-2}$ over the lower parts of the main glacier and the proglacial valley while it is underestimated by up to 25 W m$^{-2}$ over steeper slopes and ridges. The error of the modeled net turbulent flux when spatially uniform wind is assumed ((Fig. 6g–i)/(net turbulent flux from MR1) × 100), averaged separately over cells that under- or overestimate the net turbulent flux, is: (i) −38% and +38% for winter; (ii)

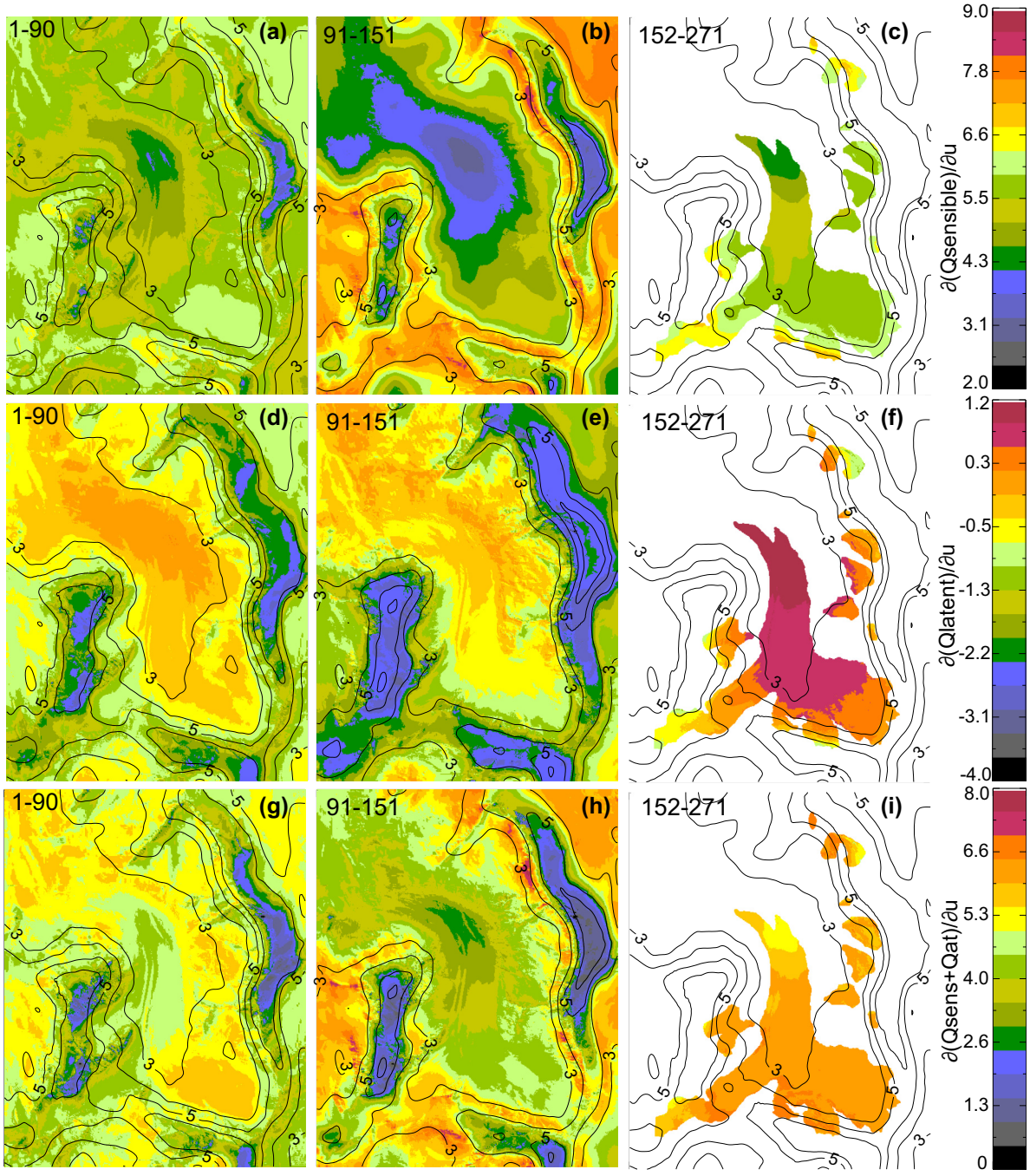


**Fig. 4.** Seasonally averaged sensitivity (MR2 - MR1) of the sensible (a–c), latent (d–f) and net (g–i) heat flux with respect to wind speed for the winter (doy: 1–90), spring (doy: 91–151) and summer (doy: 152–272) seasons, for the Haut Glacier d'Arolla in 2007. The overlaid contours show the seasonal mean wind speeds (from ARPS) that were used in MR1. For the summer season, we only discuss glacierized areas, because the non-glacierized areas become snowfree early in the season and are therefore not discussed in this study.

−43% and +58% for spring; (iii) −48% and +31% for summer (summer values contain fewer cells and no values in regions with the highest wind speed, because those regions are snow/ice-free in summer). As already mentioned, the errors depend on the location of the AWS and which part of the catchment it represents.

### 3.2.2. Model limitations

Both the energy balance model as well as the ARPS model have limitations when applied to complex terrain. The main limitations of the energy balance model, which are affecting our results, is that we assume that the mean convective and turbulent lateral fluxes are negligible. This assumption is not entirely valid because of the non-homogeneity of the flow field. In spring and summer, when the snow cover becomes patchy, the non-uniform surface temperature distribution can lead to increased advection of sensible heat, which can cause locally increased ablation rates [69,19,20]. Considering that in our winter and spring model runs we have a continuous snow cover because we did not include any snow distribution processes, the local advection due to non-uniform surface temperature distribution should be minimal. During the summer season, the local advection has strongest effects along the glacier borders, and Mott et al. [19] found that, for the

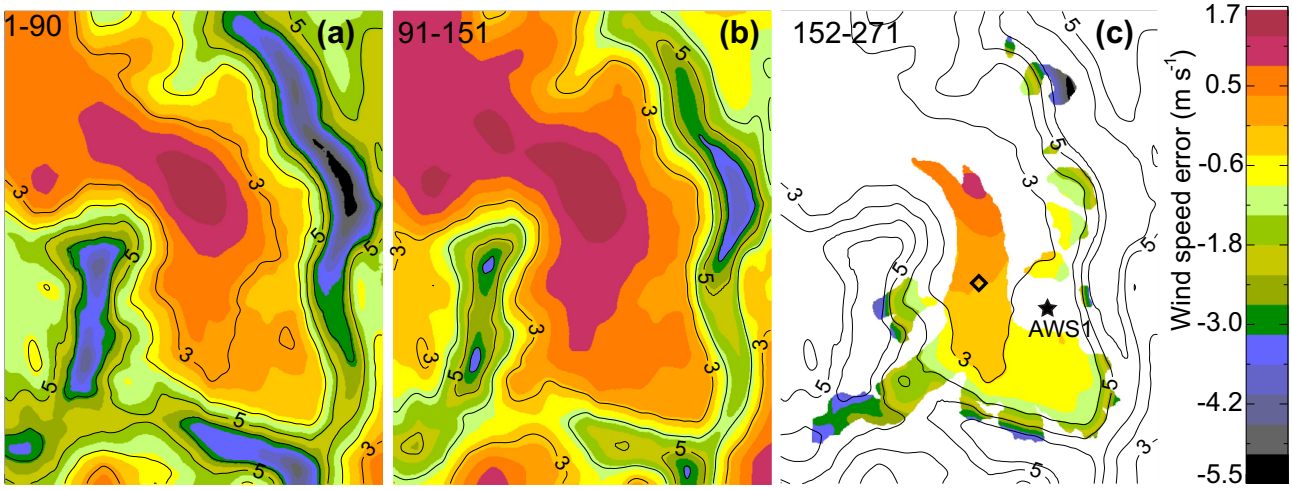


**Fig. 5.** Seasonally averaged difference between spatially uniform wind speed (MR3, Table 1) and and the modeled wind speed (MR1, from ARPS) for the winter (doy: 1–90), spring (doy: 91–151) and summer (doy: 152–272) seasons, for the Haut Glacier d'Arolla in 2007. The overlaid contours show the seasonal average of the modeled wind speed (MR1). The diamond in (c) shows the location (SA) we chose for the discussion of the sensitivity at the point scale. The star indicates the location of the automatic weather station AWS1.

average wind speed at the glacier perimeter in summer (Fig. 5c, contours), the effect of lateral heat transport is appreciable over a distance of 5–6 m, so the bulk of the glacierized area would be minimally affected through this process. The main limitation of the ARPS model is that we did not account for katabatic winds, and that the modeled wind speed is therefore likely underestimated over the glacier tongue and in the lower valley, where the katabatic winds would be strongest. This leads to an underestimation of the turbulent fluxes over the lower valley when the modeled wind speed is used. If the katabatic winds were included, the positive errors in Fig. 6g–i would become smaller. Including katabatic winds would also increase the sensitivity of turbulent fluxes over the valley floor and the main glacier (Fig. 4), where the wind speed might increase from a region of <3 m s$^{-1}$ with low sensitivity to a region of 3–6 m s$^{-1}$ with high sensitivity.

*3.2.3. Implications for energy balance modeling at the catchment scale*

Even when considering the limitations discussed above, some general implications of what locally varying wind speed means for distributed energy balance modeling can be discussed. The uncertainties associated with local wind speed variations depend on the location of the AWS that is used to drive the model and which part of the catchment it represents. However, assuming that the AWSs in mountain regions are located in the valleys and therefore underestimate wind speed over ridges and steep slopes, we can generalize some of the implications of our results for energy balance modeling at the catchment scale for different seasons: (i) Assuming spatially uniform wind speed during the *winter* season leads to over- or underestimation of turbulent fluxes, and influences the snow temperatures and sublimation, but has little impact on melt, as the temperatures are generally low (Table 1). Assuming spatially uniform wind speed can, however, significantly underestimate sublimation (or inverse sublimation) over areas with high wind speed. Enhanced sublimation causes depletion of snow over ridges and steep slopes, which already have less snow due to less preferential deposition of snow or snow drift. Sublimation (negative latent heat flux) cools the surface and can offset some of the warming from the sensible heat flux. In regions with higher relative humidity, increased turbulent fluxes can warm the surface and trigger snow melt. (ii) Assuming spatially uniform wind speed during the *spring* season leads to over- or underestimation of the snow surface temperature. During spring, the air temperature is much closer to the melting point of ice (Table 1) and and small uncertainties in turbulent fluxes can therefore increase the temperature to the melting point. The underestimation is largest over ridges and steep slopes, and the amount and timing (daily as well as seasonal timing) of spring snow melt is therefore significantly underestimated in these regions if local variations in wind speed are neglected. (iii) Assuming spatially uniform wind speed during the *summer* season leads to underestimation of turbulent fluxes over most of the glacier surface. Even if the average air temperature for summer is above freezing, the ice surface can cool below the melting point during night time due to radiative cooling. If the net turbulent flux is underestimated, the ice surface reaches the melting point later in the morning, which will lead to less modeled melt. With a higher turbulent heat flux, the ice temperature cools less during the night and the melting point is reached earlier, causing more melt. This has the largest impact on wind exposed sites.

## 4. Summary and conclusions

Wind speed analysis in mountain areas is associated with large uncertainties. Errors of wind speed estimations can influence the simulations of the timing and amount of snow- and ice-melt over complex terrain. We conducted model experiments using idealized conditions to estimate model sensitivity of turbulent fluxes and melt to wind speed for different climatic conditions. We only investigated sensitivity under stable stratification, because it is predominant over snow and ice surfaces. Our study shows that the sensitivity increases with increasing air temperature and for either extreme of relative humidity. The sensitivity of turbulent fluxes is highest when the stability parameter $\zeta = 1$ (at $u = 3$–5 m s$^{-1}$), and exponentially decreases either side of that range. That peak in sensitivity is caused by the stability correction in the turbulent fluxes parameterization, and is independent of the flux-profile relationships we applied (not shown in this work). No peak in sensitivity is modeled when neutral conditions are assumed. The wind speed range of 3–5 m s$^{-1}$, where the sensitivity of turbulent fluxes to uncertainties in wind speed is highest, is typical of many glacierized regions and can lead to large uncertainties in melt modeling. Our idealized model experiments were done assuming low insolation and $\alpha = 0.9$. Increasing insolation or

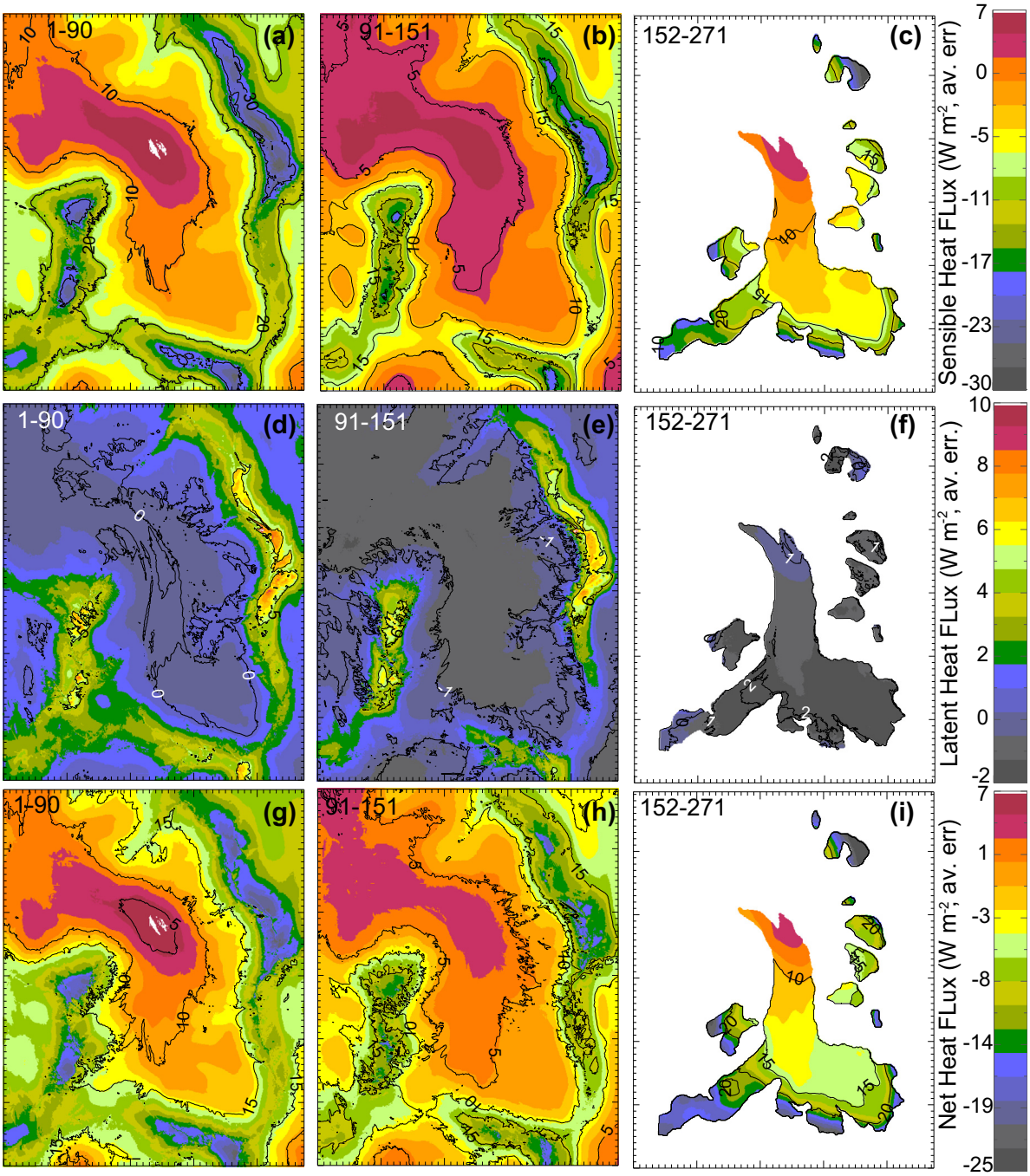


**Fig. 6.** Seasonally averaged error of turbulent fluxes for winter (doy: 1–90), spring (doy: 91–151) and summer (doy: 152–272), if spatially uniform wind speed is assumed at Haut Glacier d'Arolla in 2007. The error is calculated as the difference between the runs assuming spatially uniform wind speed (MR3) and modeled wind speed (MR1). The contours show the average heat fluxes from MR1.

decreasing albedo brings the snowpack closer to melting and therefore increases the sensitivity. Our sensitivity estimates can therefore be regarded as minimum estimates.

To estimate the uncertainties in turbulent fluxes associated with variations in wind speed in a more realistic representation of meteorological variables and evolving albedo, we ran the model for the basin of Haut glacier d'Arolla for the 2007 winter, spring and summer season using modeled wind fields as model input. The sensitivity to wind speed is largest in areas where $u = 3$–$6\ \mathrm{m\ s^{-1}}$, which confirms the results from our idealized model experiments. To quantify the error in energy balance modeling when spatially uniform wind speed is assumed, we also ran the distributed model assuming spatially uniform wind speed. The resulting turbulent flux errors when neglecting spatial variation of wind speed are highest over ridges and steep slopes (40–50%), reflecting the high uncertainty and strong local variation in wind speed in these regions. The wind speed uncertainty is likely larger than we calculate, especially over the main valley/glacier, because the regional climate model (ARPS), that we used to model wind fields, has not been set-up to allow the development of katabatic winds, which are likely to enhance the topographically modified air flow. Furthermore, because we do not model wind fields at

every timestep, but use pre-defined wind fields, our modeled temporal variations of local wind speed are too small. However, we demonstrate how the sensitivity of the turbulent fluxes could look like for a catchment in the European Alps and that the sensitivity analysis using idealized conditions can be used to estimate uncertainties in turbulent fluxes due to wind speed uncertainties in other regions as well.

It is important to note that we chose to investigate the sensitivity of energy balance modeling to uncertainties of the assumed or measured local wind speed. We did not investigate the sensitivity to air temperature and relative humidity variations despite the fact that we looked at the wind speed sensitivity in different temperature/humidity environments. The sensitivity on local variations of temperature and humidity may be subject to future research. We also want to emphasize that our results should not be interpreted as a potential reaction of the turbulent fluxes to atmospheric changes (e.g., as a consequence of climate change). In such a case, a primary change in e.g., wind speed would lead to temperature and humidity changes in the atmospheric boundary layer and therefore those non-local feed-backs would have to be considered. Our results should be interpreted as the potential modeling error if the local wind speed is not known or has uncertainties. Our results therefore help to better quantify the often discussed sensitivity (e.g., [70]) of energy balance models on (high quality) input data and provide the way to improve the application of energy balance models in particular in complex terrain.

## Acknowledgments

We thank Javier G. Corripio for providing the energy balance model SnowDEM and for his help with the model and Paolo Burlando for providing the framework for research on the Haut Glacier d'Arolla. This manuscript was improved through numerous discussions with Huw Horgan and by the constructive comments of two anonymous reviewers. Funding for this research has been provided by the Swiss National Science Foundation (R. Dadic, R. Mott) and the Center for Environment and Sustainability CCES (SwissEx: R. Mott).

## References

[1] Pomeroy JW, Gray DM, Landine PG. The Prairie Blowing Snow Model: characteristics, validation, operation. J Hydrol 1993;144:164–92.
[2] Liston GE, Sturm M. A snow–transport model for complex terrain. J Glaciol 1998;44(148):498–516.
[3] Lehning M, Löwe H, Ryser M, Raderschall N. Inhomogeneous precipitation distribution and snow transport in steep terrain. Water Resour Res 44 (7), 10.1029/2007WR006545.
[4] Dadic R, Mott R, Lehning M, Burlando P. Wind influence on snow depth distribution and accumulation over glaciers. J Geophys Res 115 (F01012), 10.1029/2009JF001261.
[5] Mott R, Lehning M. Meteorological modeling of very high resolution wind fields and snow deposition for mountains. J Hydrometeorol 2010;11(4):934–49. http://dx.doi.org/10.1175/2010JHM1216.1.
[6] Schneiderbauer S, Prokop A. The atmospheric snow-transport model: SnowDRIFT3D. J Glaciol 2011;57(203):526–42.
[7] Dery SJ, Taylor PA, Xiao J. The thermodynamic effects of sublimating, blowing snow in the atmospheric boundary layer. Boundary–Layer Meteorol 1998;89:251–83.
[8] Pomeroy J, Essery R. Turbulent fluxes during blowing snow: field tests of model sublimation predictions. Hydrol Process 1999;19(18):2963–75.
[9] Liston G, Sturm M. Winter precipitation patterns in Arctic Alaska determined from a blowing-snow model and snow-depth observations. J Hydrometeorol 2002;3:646–59.
[10] Strasser U, Bernhardt M, Weber M, Liston G, Mauser W. Is snow sublimation important in the alpine water balance? Cryosphere 2008;2(1):53–66.
[11] MacDonald M, Pomeroy J, Pietroniro A. On the importance of sublimation to an alpine snow mass balance in the Canadian Rocky Mountains. Hydrol Earth Syst Sci 2010;14(7):1401–15. http://dx.doi.org/10.5194/hess-14-1401-2010.
[12] Groot Zwaaftink S, Löwe H, Mott R, Bavay M, Lehning M. Drifting snow sublimation: a high resolution 3-D model with temperature and moisture feedbacks. J Geophys Res 116 (D16107), 10.1029/2011JD015754.
[13] Male D, Granger R. Snow surface energy exchange. Water Resour Res 1981;17:609–27.
[14] Greuell W, Oerlemans J. Sensitivity studies with a mass balance model including temperature pofile calculations inside the glacier. Zeitsch Glestcherkinde Glazialgeol 1986;22(2):101–24.
[15] Marks D, Dozier J. Climate and energy exchange at the snow surface in the alpine region of the Sierra Nevada. 2. Snow cover energy balance. Water Resour Res 1992;28(11):3043–54.
[16] Marks D, Winstral A. Comparison on snow deposition, the snow cover energy balance, and snowmelt at two sites in a semiarid mountain basi. J Hydrometeorol 2001;2(3):213–27.
[17] Pohl S, Marsh P, Liston G. Spatial-temporal variability in turbulent fluxes during spring snowmelt. Arctic, Antarctic Alpine Res 2006;38(1): 136–46.
[18] Fujita K, Hiyama K, Iida H, Ageta Y. Self-regulated fluctuations on the ablation of a snow patvh over four decades. Water Resour Res 46 (W11541).
[19] Mott R, Egli E, Grünewald T, Dawes N, Manes C, Bavay M, Lehning M. Micrometeorological processes driving snow ablation in an Alpine catchment. The Cryosphere 2011;5:1083–1098. 10.5194/tcd-5-2159-2011.
[20] Mott R, Gromke C, Grünewald T, Lehning M. Relative importance of advective heat transport and boundary layer decoupling in the melt dynamics of a patchy snow cover. Adv Water Resour 2013;55:88–97.
[21] Marks D, Kimball J, Tingey D, Link T. The sensitivity of snowmelt processes to climate conditions and forest cover during rain-on-snow: a case study of the 1996 Pacific Northwest flood. Hydrol Process 1998;12:1569–1587.
[22] Mott R, Gromke C, Grünewald T, Lehning M. Relative importance of advective heat transport and boundary layer decoupling in th emelt dynamics of a patchy snow cover. Adv Water Resour 2013;55:88–97.
[23] Kuhn M. The mass balance of very small glaciers. Zeitschrift für Glestcherkunde und Glazialgeologie 1995;31:171–9.
[24] Hoffmann MJ, Fountain AG, Achuff JM. 20th–century variations in area of cirque glaciers and glacierets. Rocky Mountain National Park, Rocky Mountains, Colorado, USA, Annals of Glaciology 2007;46:349–54.
[25] Winstral A, Marks D. Simulating wind fields and snow redistribution using terrain-based parameters to model snow accumulation and melt over a semi-arid mountain catchment. Hydrol Process 2002;16(18):3585–603.
[26] Monin A, Yaglom A. Statistical fluid mechanics: mechanics of turbulence, vol. 1. Cambridge, MA: MIT Press; 1971. p. 769.
[27] Mahrt L. Stratified Atmospheric Boundary Layers and Breakdown of Models. Theoret Comput Fluid Dyn 1998;11:263–79.
[28] Pleim J. A simple, efficient solution of flux-profile relationships in the atmospheric surface layer. J Appl Meteorol Climatol 2006;45:341–7.
[29] Deardorff J. Dependence of air-sea transfer coeffinients on bulk stability. J Geophys Res 1968;73(8):2549–57.
[30] Webb E. Profile relationships: The log-linear range, and extension to strong stability. Quart J Roy Meteorol Soc 1970;96:67–90.
[31] Kondo J, Kanechika O, Yasuda N. Heat and momentum transfers under strong stability in th eatmospheric surface layer. J Atmos Sci 1978;35:1012–21.
[32] Jordan R, Andreas E, Makshtas A. Heat budget of snow covered sea ice at North Pole 4. J Geophys Res 1999;104(C4):7785–7806.
[33] Stössel F, Guala M, Fierz C, Manes C, Lehning M. Micrometeorological and morphological observations of surface hoar dynamics on a mountain snow cover. Water Resour Res 46 (W04511), 10.1029/2009WR008198.
[34] Brutsaert W. Evaporation into the atmosphere: theory, history and applications. D. Reidel Publishing Co., 1982.
[35] Corripio JG. Modelling the energy balance of high altitude glacierised basins in the Central Andes, PhD thesis. The University of Edinburgh; 2002.
[36] Dadic R, Corripio JG, Burlando P. Mass balance estimates for Haut Glacier d'Arolla from 2000–2006 using DEM/s and Distributed Mass Balance Modeling. Ann Glaciol 2008;49:22–6.
[37] Dadic R, Mott R, Lehning M, Burlando P. Parametrization for wind-induced preferential deposition of snow. Hydrol Process 24, 10.1002/hyp.7776.
[38] Pellicciotti F, Helbing J, Rivera A, Favier V, Corripio JG, Araos J, et al. A study of the energy balance and melt regime on Juncal Norte Glacier, semi-arid Andes of central Chile, using melt models of different complexity. Hydrol Process 2008;22:3980–97. http://dx.doi.org/10.1002/hyp.7085.
[39] Stull R. An introduction to boundary layer meteorology, ISBN 90-277-2768-6. Kluwer Academic Publishers; 1988.
[40] Monin A, Obukhov A. Basic laws of turbulent mixing in the surface layer of the atmosphere. Tr Akad Nauk SSSR Geophiz Inst 1954;24:163–87.
[41] Panofsky HA. Determination of stress from wind and temperature measurements. Quart J Roy Meteorol Soc 1963;89(379):85–94.
[42] Dyer AJ. A review of flux-profile relationships. Boundary–Layer Meteorol 1974;7(3):363–72.
[43] Yaglom A. Comments on wind and temperature flux-profile relationships. Boundary–Layer Meteorol 1977;11:89–102.
[44] Andreas E. Parameterizing scalar transfer over snow and ice: A review. J Hydrometeorol 2002;3(4):417–32.
[45] Businger JA. Transfer of momentum and heat in the planetary boundary layer. In: Proc Symp Arctic Heat Budget and Atmos Circulation, RAND Corp. RM-5233-NSF, 1966. p. 305–32.
[46] Dyer A, Hicks B. Flux-gradient relationships in constant flux layer. Quart J Roy Meteorol Soc 1970;96(410):715–21.
[47] Zilitinkevich S, Chalikov D. On the determination of the universal wind and temperature profiles in the surface layer of the atmosphere, Izv. Acad. Sci. USSR, Atmos. Oceanic Phys. 1968;4:915–29.

[48] Businger JA, Wyngaard JC, Izumi Y, Bradley EF. Flux-profile relationships in atmospheric surface layer. J Atmos Sci 1971;28(2):181–9.
[49] Hicks B. Wind profile relationships from the Wangara experiments. Quart J Roy Meteorol Soc 1976;102:535–51.
[50] Garratt J. The atmospheric boundary layer. Cambridge University Press; 1992.
[51] Sharan M. performance of various similarity functions for nondimensional wind and temperature profiles in the surface layer in stable conditions. Atmos Res 2009;94:246–53.
[52] Mahrt L. Stratified atmospheric boundary layers. Boundary–Layer Meteorol 1999;90:375–96.
[53] Mahrt L. Intermittency of the atmospheric boundary layer. J Atmos Sci 1989;46:79–95.
[54] Beljaars A, Holtslag A. Flux parameterization over land surfaecs for atmospheric models. J Appl Meteorol 1991;30:327–41.
[55] Cheng Y, Parlange M, Brutsaert W. Pathology of Monin–Obukhov similarity in the stable boundary layer. J Geophys Res 110 (D6), 10.1029/2004JD004923.
[56] Lettau H. Wind and temperature profile prediction for diabatic surface layers including strong inversion cases. Boundary–Layer Meteorol 1979;17:443–64.
[57] Holtslag A, de Bruin H. Applied modeling of the nighttime surface energy balance over land. J Appl Meteorol 1988;27:689–704.
[58] Cheng Y, Brutsaert W. Flux-profile relationships for wind speed and temperature in the stable atmospheric boundary layer. Boundary–Layer Meteorol 2005;114:519–38.
[59] Grachev A, Andreas E, Fairall C, Guest P, Persson P. SHEBA flux-profile relationships in the stable atmospheric boundary layer. Boundary–Layer Meteorol 2007;124:315–33.
[60] Jacobson M. Fundamentals of atmospheric modeling. Cambridge University Press; 1999.
[61] Plüss C, Mazzoni R. The role of turbulent heat fluxes in the energy balance of high Alpine snow cover. Nordic Hydrol 1994;25(1–2):25–38.
[62] Brock BW, Willis IC, Sharp MJ. Measurement and parametrisation of aerodynamics roughness lenth variations at Haut Glacier d'Arolla, Switzerland. J Glaciol 2006;52(177):1–17.
[63] Xue M, Droegemeier KK, Wong V, Shapiro A, Brewster K, Carr F, Weber D, Liu Y, Wang D. The Advanced Regional Prediction System (ARPS) – Part II: model physics and applications. Meteorol Atmos Phys 2001;76:143–65.
[64] Raderschall N, Lehning M, Schaer C. Fine-scale modelling of the boundary-layer wind field over steep topography. Water Resour Res 44 (9).
[65] Lehning M, Bartelt P, Brown R, Russi R, St'ockli U, Zimmerli M, Snowpack model calculations for avalanche warning based upon a network of weather and snow stations. Cold Region Sci Technol 1999;30:145–157.
[66] Corripio JG. Vectorial algebra algorithms for calculating terrain parameters from DEMs and solar radiation modeling in mountainous terrain. Int J Geographic Inform Sci 2003;17(1):1–23.
[67] Dadic R. Monitoring and modeling snow accumulation processes in glacierized Alpine basins. PhD thesis, ETH Zürich, http://e-collection.ethbib.ethz.ch/view/eth:31154, URL http://e-collection.ethbib.ethz.ch/view/eth:31154, 2008
[68] Gillet S, Cullen N. Atmospheric controls on summer ablation over Brewster Glacier, New Zealand. Int J Climatol, 10.1002/joc.2216.
[69] Liston GE. Local advection of momentum, heat and moisture during the melt of patchy snow covers. J Meteorol 1995:1705–15.
[70] He M, Hogue T, Franz K, Margulis S, Vrugt J. Corruption of parameter behavior and regionalization by model and forcing data errors: a Bayesian example using the SNOW17 model. Water Resour Res 47 (W07546), 10.1029/2010WR009753.